



Fluorescent matter in the eastern Atlantic Ocean. Part 2: vertical profiles and relation to water masses

S. DETERMANN,* R. REUTER*† and R. WILLKOMM*

(Received 7 July 1993; in revised form 8 March 1995; accepted 25 September 1995)

Abstract—Water samples taken at seven stations in the eastern Atlantic Ocean were fluorometrically analyzed. Vertical profiles describe the distribution of gelbstoff and of tyrosine-like and tryptophan-like molecules. These are compared with hydrographic data. Gelbstoff fluorescence is low near the sea surface due to photodegradation. Except for enhanced values at 300–500 m depth at some stations, Gelbstoff fluorescence is almost constant in intermediate (Mediterranean Water, Antarctic Intermediate Water) and deep waters (North Atlantic Deep Water) despite the very different origins of these water masses.

In contrast to gelbstoff, tryptophan- and tyrosine-like signals are highest near the sea surface. Particulate organic matter and derived dissolved organic molecules are discussed as possible sources of these fluorophores. In the upper portion of the main thermocline, where the gelbstoff is greater than deeper in the water column, the fluorescence signals of gelbstoff and tryptophan-like molecules covary. This supports the assumption that decomposition of sinking particles, and increased concentrations of bacteria due to this process, contribute to the vertical distribution of fluorescent matter at these depths. Copyright © 1996 Elsevier Science Ltd

INTRODUCTION

For the ANT-VIII/7 cruise of R.V. *Polarstern* the ship sailed from Capetown, South Africa (1 May 1990), to Bremerhaven, Germany (22 May 1990) (Fütterer and Schrems, 1991). Water samples were taken at 14 m depth along the ship track, by use of a snorkel system installed in the hydrographic well of the ship, and fluorometrically analyzed. The results of these underway measurements were presented in Part 1 of this paper (Determann *et al.*, 1994).

In addition to these measurements in the mixed layer, seven stations were occupied at locations shown in Fig. 1 and Table 1. Depth profiles of hydrographic properties were measured, and water samples were taken for the laboratory analysis of biological and chemical parameters and for fluorescence analyses. The purpose of this paper is to report on the depth distribution of fluorescent matter at these locations in the eastern Atlantic Ocean, and on the relationship of fluorescent matter to other water column parameters.

*Carl von Ossietzky Universität Oldenburg, Fachbereich Physik, 26111 Oldenburg, Germany.

†Author to whom correspondence should be addressed.

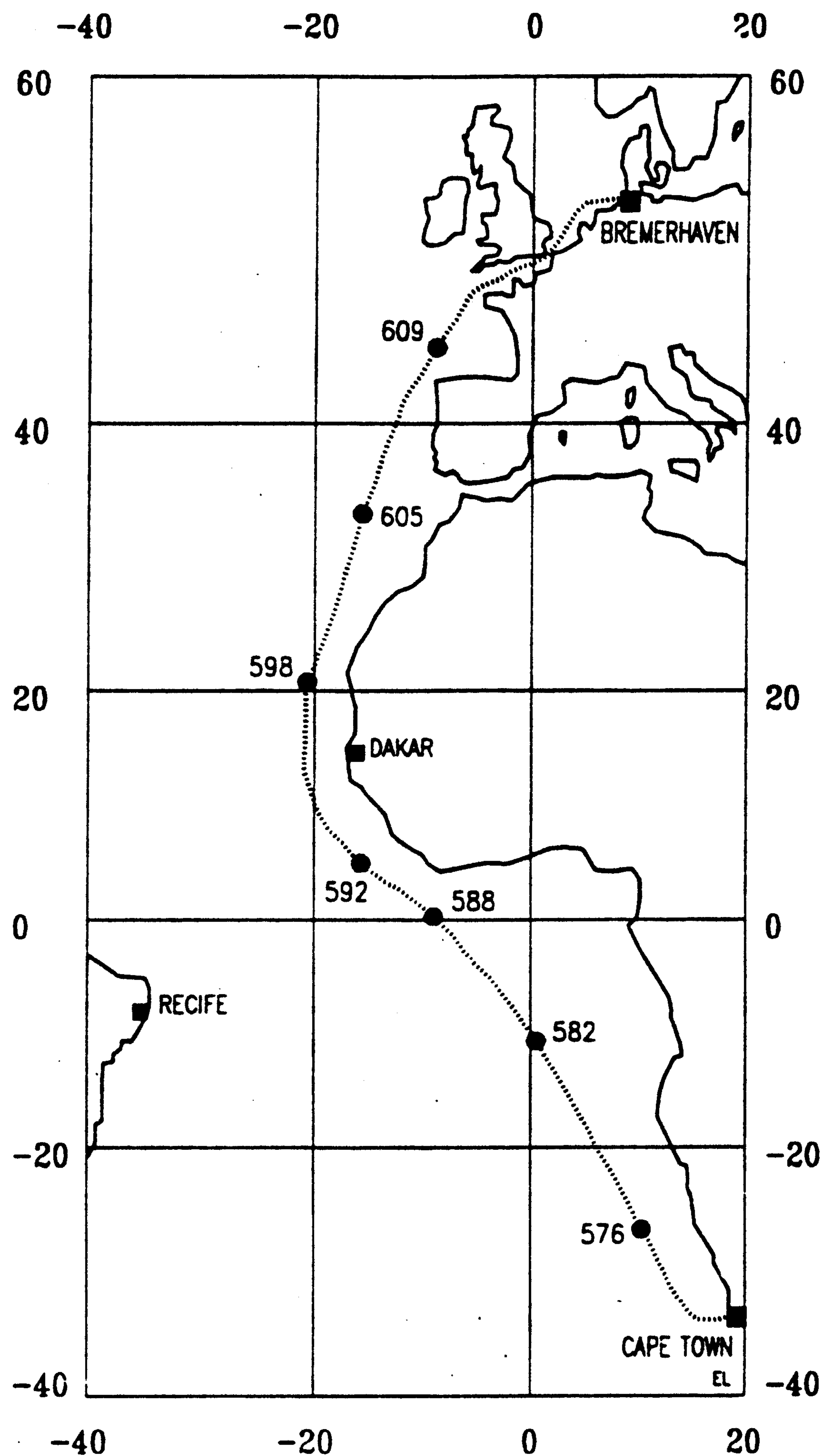


Fig. 1. Cruise track of R.V. *Polarstern* during ANT VIII/7, 22 May 1990. Circles denote the positions of stations (Table 1).

METHODS

Sampling

Water samples were taken at 12 depths with a rosette sampler using 12 l Niskin bottles. A Seabird probe was mounted on the sampler for CTD and oxygen measurements. Since Seabird probe data were stored internally instead of being transmitted to a deck unit, on-line information on hydrographic parameters was not available. Therefore, depths of water sampling given below indicate cable lengths.

Samples were taken for onboard analysis at 5, 20, 50, 100, 200, 300 and 500 m depth in the upper water column, and at 500–1000 m intervals in intermediate and deep waters. Since

Table 1. Dates and geographical positions of stations during cruise ANT-VIII/7 of R.V. Polarstern, May 1990. A listing of the surface stations, and hydrographic data are found in Fütterer and Schrems (1991)

Station	Date	Position		Water Depth (m)/max. Sampling Depth (m)
576 Cape Basin	3 May 1990	27°17.8'S	10°38.7'E	4795/3000
582 Angola Basin	6 May 1990	13°27.7'S	2°16.0'E	5581/3500
588 Guinea Basin	9 May 1990	0°31.1'S	8°00.9'W	4951/3000
592 Sierra Leone Basin	11 May 1990	5°59.4'N	16°20.2'W	4933/4800
598 Cape Verde Basin	14 May 1990	20°36.4'N	20°27.2'W	3889/3000
605 Mediterranean outflow	17 May 1990	35°58.2'N	14°35.5'W	4223/4000
609 Biscay	19 May 1990	44°47.0'N	8°53.8'W	4864/4600

sampling with high resolution within the upper 300 m was given high priority, the maximum sampling depth was in some cases limited to 1000–2000 m above the seafloor. CTD profiling was done on the downcast, and water sampling was done during recovery. Although this can give rise to errors if CTD data are related to water sampling data in highly stratified layers, the Niskin bottles were well rinsed in this way before water samples were taken, which reduces the risk of contamination with organic material, e.g. from microlayers on the sea surface.

Unfiltered samples were fluorometrically analyzed with a single run for each sample, instead of the extended procedure using three cuvettes for surface sample analyses described in Determann *et al.* (1994). This was necessary to perform the analysis in the shortest possible time after sampling, which was not more than 1 h. Hence, outliers due to possible sample contamination cannot be identified and discarded from the data set. Fluorescence efficiencies are generally dependent on temperature. Therefore, samples from below the near-surface layer were kept at 5°C during the measurement, by using an instrumental cooling assembly to keep temperatures at about the *in situ* value. This will allow the data to be related to future multi-wavelength *in situ* measurements (Heuermann *et al.*, 1995).

Excitation and emission wavelengths used for the fluorescence measurements, made with a Perkin Elmer LS50 Luminescence Spectrometer, are given in Table 2, together with the types of substances associated with these fluorescence data. At Stations 576 and 582, the measurements did not include the 230 nm excitation wavelength, and hence no data for tyrosine-like fluorescence are available from these positions. With these exceptions, storage and handling of samples, experimental methods and their accuracies are the same as described in Determann *et al.* (1994).

As described in the earlier paper, fluorescence spectra are calibrated by normalization to the integrated water Raman scattering band, yielding the Raman unit as a quantitative measure of the signal intensity. With an appropriate choice of the range of detection

Table 2. Spectral parameters of fluorescence measurements with a Perkin Elmer LS50 Luminescence Spectrometer

Excitation (nm)	Emission Range (nm)	Suggested Substance Type at peak emission wavelength (nm)
230	240–430	Tyrosine at 280...300 (290,5) Tryptophan at 325...350 (330,5)
254	260–500 400–700*	Tryptophan at 320...350 (320,1) Gelbstoff at 440...460 (440,2)
270	280–500	Tryptophan at 325...350 (320,1) Gelbstoff at 440...460 (440,2)

Substance types and emission wavelengths chosen for their identification are given. Values in brackets denote centre wavelengths and bandwidths used for off-line intensity readings. Spectral excitation and emission bandwidths: 7 nm. A spectral calibration of the instrument has been performed as described in Determann *et al.* (1994).

*A 350 nm long-wave pass filter in front of the emission monochromator suppresses second order diffraction signals.

wavelengths, water Raman scattering is inherently included in each spectrum. Therefore, this procedure is of great advantage compared to the use of fluorescence standards like quinine sulfate, which would require a separate measurement for each calibration of the instrument. The relation of Raman units to some quinine sulfate standards reported in the literature is given in Table 3.

RESULTS

Depth profiles

The depth profiles obtained at Stas 582 in the Angola Basin, 592 in the Sierra Leone Basin, and 609 in the Bay of Biscay are given in Figs 2–4. The graphs display profiles of gelbstoff fluorescence (excitation/emission: 254 nm/440 nm), and fluorescence of tryptophan-like (270 nm/320 nm) and tyrosine-like (230 nm/290 nm) substances, in relation to temperature, salinity, oxygen and nutrients. The vertical structure of CTD and fluorescence data at Stas 576 and 588 were similar to those observed at Sta. 582. The same holds for the profiles of Stas 598 and 605, which were comparable to those at Stas 592 and 609, respectively. Therefore, these data are not displayed graphically. Numerical listings of the complete data set are given in the appendix.

Gelbstoff fluorescence

The depth profiles of gelbstoff fluorescence (254 nm/440 nm) were characterized by very low signal intensities in the surface layer, ranging between 2 and 3×10^{-3} nm⁻¹ Raman units at 5 m depth. At a few stations this layer extended down to the 20 m sampling depth. These data agree well with the results of the the near-surface sampling programme (Determann *et al.*, 1994: their Fig. 5), where the same values were found.

Table 3. Comparison of fluorescence standards based on quinine sulfate with Raman units

Notation	Signal intensity	(a) Fluorophor concentration solvent	(a) ex/em wavelength ex/em bandwidth	Reference	Relation to Raman units
Milli Fluoreszenz [mFl]	73 mFl	0.1 mg/l quinine bisulfate* 0.01 N H ₂ SO ₄	365/460 nm 7†/10† nm	Kalle (1963)	1 mFl \equiv 11.0×10^{-3} nm ⁻¹ †
Fluorescence units [flu]	30 flu	28.0 µg/l quinine sulfate* H ₂ SO ₄ †, pH 2.0	340/440 nm 7†/10† nm	Dorsch and Bidleman (1982)	1 mFl \equiv 8.6×10^{-3} nm ⁻¹
Fluorescence units [flu]	25 flu	2.8 µg/l quinine sulfate HClO ₄ †, pH 2.0	320/420 nm 10/10 nm§	Hayase <i>et al.</i> (1987)	1 mFl \equiv 0.67×10^{-3} nm ⁻¹
Fluorescence units [flu]	45 flu	2.8 µg/l quinine sulfate mono-hydrate*, H ₂ SO ₄ †, pH 2.0	325/450 nm laser line/20 nm¶	Chen and Bada (1992)	1 flu \equiv 3.2×10^{-3} nm ⁻¹
Quinine sulfate unit [QSU]	1 QSU	1 ppb quinine sulfate 0.05 M H ₂ SO ₄	350/450 nm 7†/10† nm	Mopper and Schultz (1993)	1 QSU \equiv 0.48 nm ⁻¹ †

Measurements were performed with the Perkin Elmer LS50 luminescence spectrometer used onboard R.V. *Polarstern*. Experimental conditions were taken from the cited literature and reproduced. Measurements were made at room temperature. The relative error of the calculated relation to Raman units is estimated to < 10%.

*Quinine sulfate dihydrate used in our measurement, with quinine sulfate concentration in solution as given in the reference.

†Not specified in reference.

‡Water Raman was measured separately in purified water because of overlap with the intense quinine sulfate fluorescence band.

§7/10 m in our measurement; a change of bandwidths does not affect the result since the integrated water Raman band remains invariant.

¶5/20 nm in our measurement.

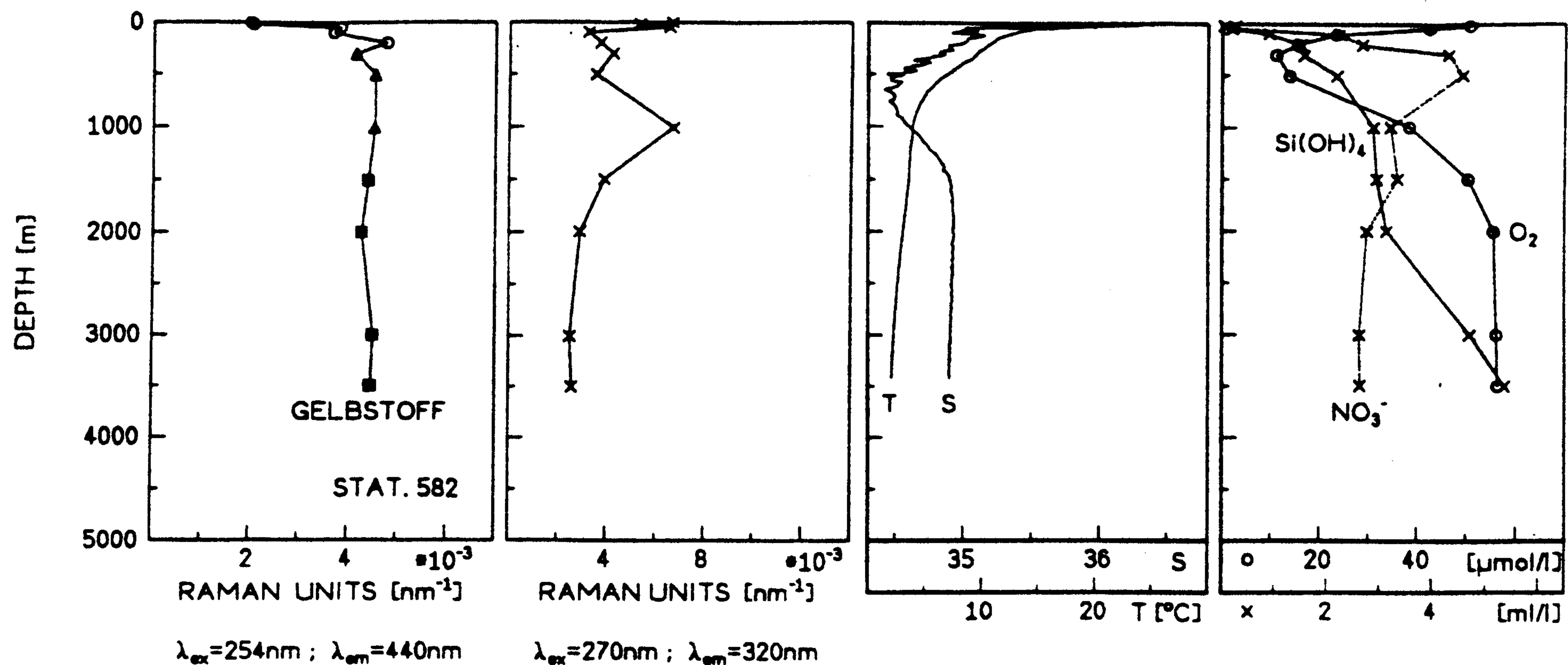


Fig. 2. Station 582, 'Angola Basin'. Profiles of gelbstoff fluorescence at 440 nm with 254 nm excitation wavelength, tryptophan-like fluorescence with 270 nm excitation and 320 nm emission, potential temperature and salinity, nutrients and oxygen. See Fig. 5 for an explanation of symbols used in the Gelbstoff profile. Profiles of temperature, salinity and chemical parameters are partly unpublished data made available by A. Michel, Alfred Wegener Institute, Bremerhaven, Germany (Michel, 1991).

Except for Stas 605 and 609, where near-surface samples were not gathered, a strong gradient was observed between the surface layer and 50 m water depth, with signal intensities typically increasing by 50–100% of the surface value. At Stas 588, 592 and 609 a maximum at 200–300 m depth was observed. The structure at Sta. 576 in the Cape Basin was different; there a minimum of gelbstoff fluorescence was found at 200 m depth, with increasing signals below. The variability of the signal at Stas 582, 598 and 605 was smaller at these water depths, near the limit of the experimental resolution, which is estimated to be better than 20% for these measurements (Determann *et al.*, 1994).

The fluorescence of intermediate and deep waters at depths of more than 500 m was very

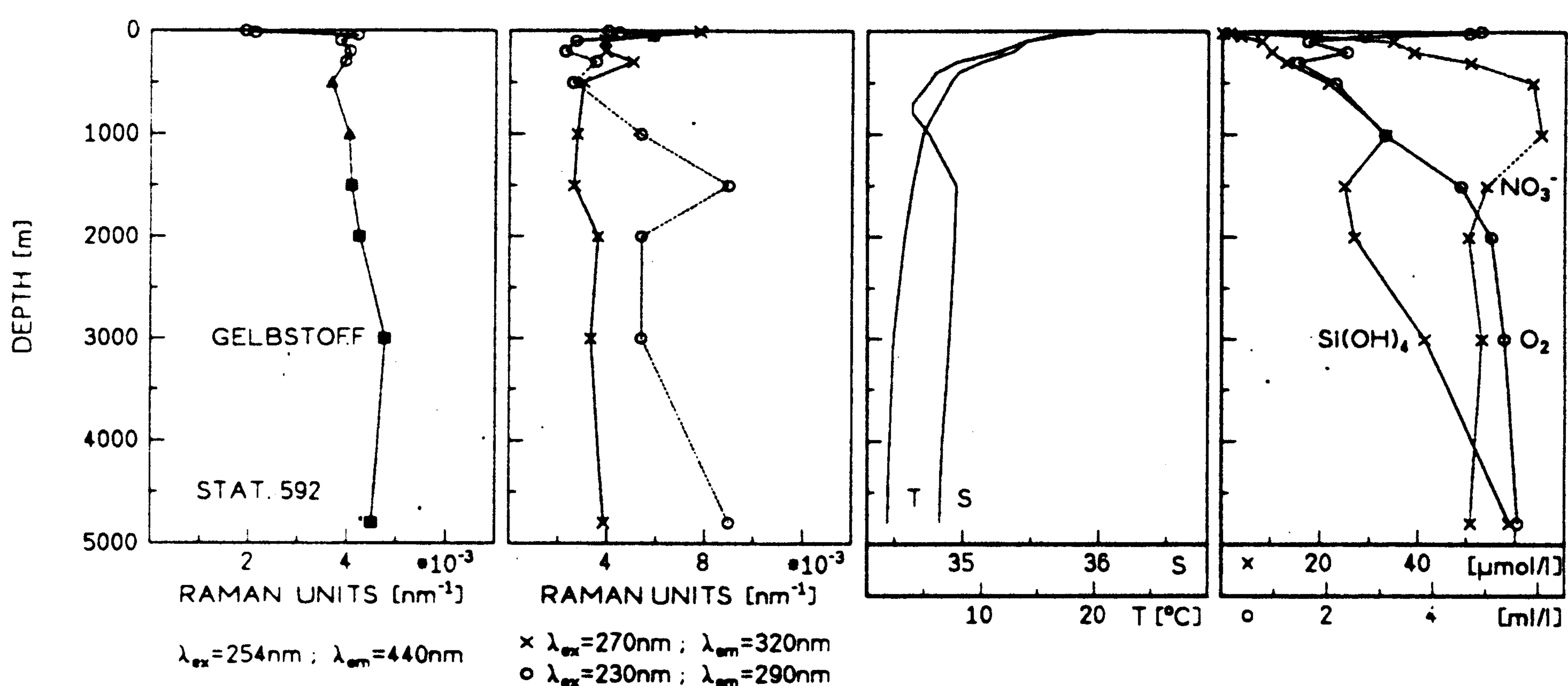


Fig. 3. Station 592, 'Sierra Leone Basin'. Same parameters as in Fig. 2, with the addition of the profile of tyrosine-like fluorescence with 230 nm excitation and 290 nm emission. Temperature and salinity readings were taken from a graphic printout since the original data file is no longer available. Therefore, the fine structure of the salinity profile within the thermocline, similar to Fig. 2, is not resolved.

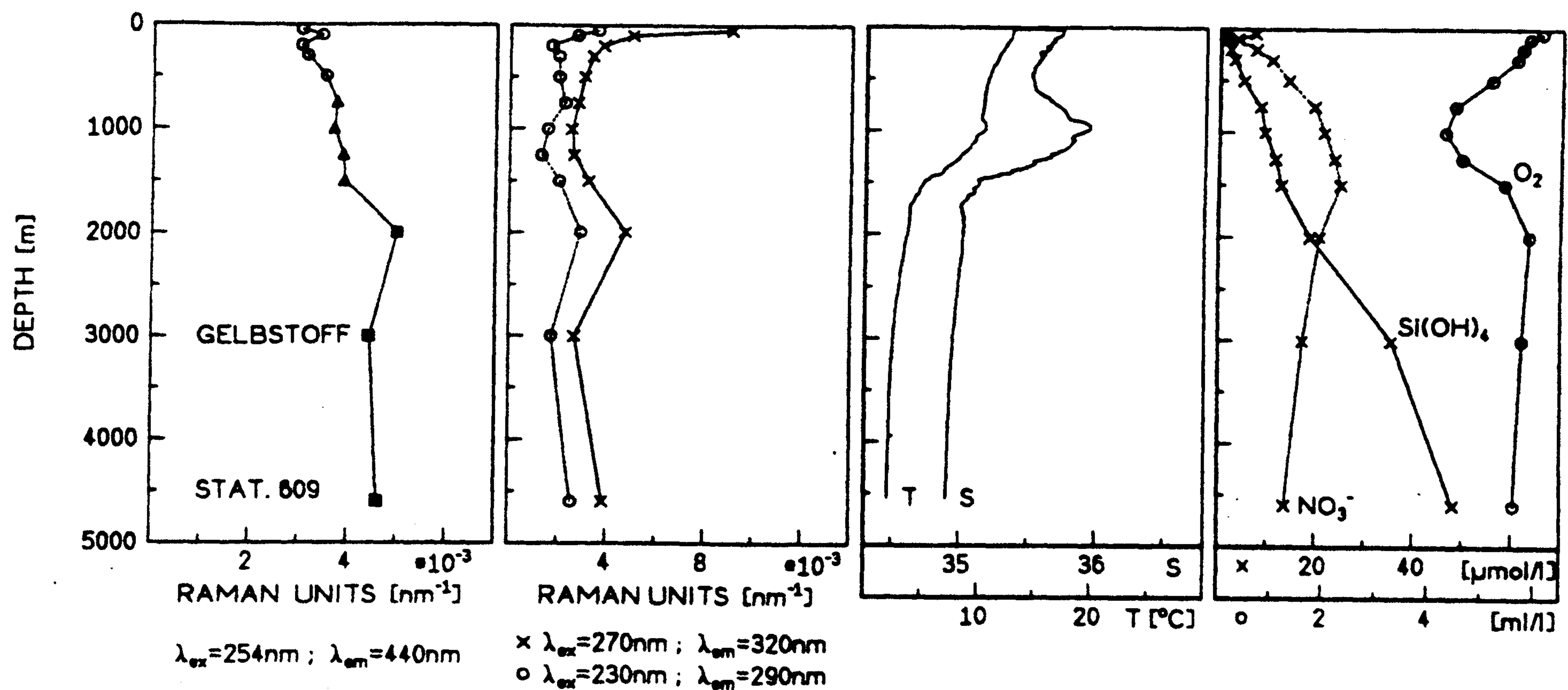


Fig. 4. Station 609, 'Biscay'. Notation as Figs 2 and 3.

homogeneous, with a typical value of $4 \times 10^{-3} \text{ nm}^{-1}$ Raman units. A few local increases, e.g. Sta. 609 at 2000 m depth (Fig. 4), might be outliers due to a possible contamination of these samples.

Tryptophan-like and tyrosine-like fluorescence

The vertical distribution of fluorescence signals that are attributed to the aromatic amino acids tryptophan (270 nm/320 nm) and tyrosine (230 nm/290 nm), or to their derivatives, differed from the gelbstoff profiles. Tryptophan-like fluorescence was very high, at about $7\text{--}9 \times 10^{-3} \text{ nm}^{-1}$ Raman units, in the upper water layer. This layer with increased signal intensities extended down to about 50 m depth, which was approximately twice as deep as the surface layer with low gelbstoff fluorescence. From the surface layer down to 500 m depth the tryptophan profiles were highly variable. Intermediate and deep waters displayed a virtually constant fluorescence signal of about $3\text{--}4 \times 10^{-3} \text{ nm}^{-1}$ Raman units, except for a few local maxima which might again be due to contamination.

Tyrosine-like fluorescence was of the same order of magnitude as that due to tryptophan. However, the pronounced maximum in the surface layer was not present. At greater depths the shapes of certain tyrosine profiles were similar to those of the tryptophan profiles. The tyrosine signal was very high at a few locations and water depths, and this effect is not yet understood. Despite the risk of unidentified contamination effects, we do not consider the tyrosine fluorescence signal and its occasionally high values as simple artifacts. An organic contamination of sample or cuvette during handling, e.g., a fingerprint on the cuvette surface, would result in a drastic increase of fluorescence emission in the 350 nm region, with excitation below 300 nm, which is not the case here.

DISCUSSION

Gelbstoff near the sea surface

The low values of gelbstoff fluorescence near the sea surface are due to photodegradation of fluorescent compounds by sunlight in the photic zone, which is a well-known

phenomenon (Ivanoff, 1973; Kramer, 1979; Nyquist, 1979; Bristow and Nielsen, 1981; Hayase *et al.*, 1987, 1988; Ertel, 1990; Kouassi and Zika, 1990a, Kouassi *et al.*, 1990b; Mopper *et al.*, 1991). The poor stability of fluorescent compounds with respect to sunlight, particularly the UV-B portion of the spectrum (Kieber *et al.*, 1990), explains the depletion of the signal in the upper 20 m of the water column (Figs 2–4). The low signal intensity in the surface layer of the Black Sea found by Coble *et al.* (1991) is interpreted in the same way. Very similar depth profiles of gelbstoff fluorescence have been reported by Chen and Bada (1992) for the same thickness of the surface layer in various regions of the central North Pacific and in the Sargasso Sea. These authors conclude that the upper 10–20 m of the water column correspond to the penetration depth of photoreactive light, and the photobleached fluorescent compounds are then wind-mixed through the upper 50 m of the ocean.

In our data, the magnitude of the fluorophore reduction near the sea surface is on the order of 30–70% compared to the concentration at the lower edge of the mixed layer where the intensity of sunlight is low. Since photobleaching in open ocean waters seems to be a rapid effect, with timescales of 1 h–1 day, the short-term history and values of the light conditions and vertical eddy diffusivity are factors which determine the shape of the depth profile in the upper water column (Kouassi *et al.*, 1990b). Accordingly, photobleaching should be more pronounced at low latitudes, because of stronger sunlight and higher stability of the near-surface layer, when compared to mid- and high-latitudes. Our depth profiles support this statement.

It follows that the influence of light-induced bleaching on water samples at 14 m depth, which were collected with the ship underway, is difficult to estimate. At Stas 576, 582 and 592 the gelbstoff data at 5 and 20 m sampling depths are virtually identical. At Stas 588 and 598 photobleaching is not apparent at 20 m depth. Hence the underway samples taken in the same regions of the ship track were collected in a zone with a high vertical gradient of the gelbstoff fluorescence profile, and sampling closer to the sea surface would probably have yielded systematically lower fluorescence values than reported previously (Determann *et al.*, 1994).

Low values of gelbstoff fluorescence near the sea surface were also found by Mopper and Schultz (1993) in the Sargasso Sea. However, the signal increases in these profiles by a factor of two, almost linearly with depth down to about 200 m, which is deeper than the photoreactive surface layer. *T/S* data are not given by these authors, but we assume that the wind-mixed-layer depth is shallower than 200 m. This would suggest that mechanisms other than the direct influence of photobleaching and subsequent mixing led to the vertical structure in these data. A process which produces very similar vertical structures in our data is discussed in the next section.

Gelbstoff in the upper water column

Except for Stas 576 and 605, maxima are found at 200–300 m depth, in the upper portion of the main thermocline. These maxima are particularly evident at Stas 582, 588 and 598, i.e. in the highly productive upwelling regions of the Benguela and Canary Current, and at Sta. 609 in the Bay of Biscay, where biological productivity is also high (Berger, 1992). The maximum is also less pronounced in the region of the Equatorial Counter Current, Sta. 592, where the productivity is lower. This pattern leads to the hypothesis that the maximum of fluorescent DOM at 200–300 m depth is a consequence of biological productivity in the euphotic zone.

It is useful to compare the gelbstoff profiles with chemical parameters. The mid-depth fluorescence maximum is particularly found at stations with low oxygen values at intermediate water depths, i.e. with O_2 values of less than 2 ml l^{-1} . The depth of the fluorescence maximum is above the oxygen minimum, not coincident with it. Apparently the oxygen minimum is not induced by degradation of sinking particles, if the depth of highest degradation and fluorophore release are the same. Overall, the role of the intermediate oxygen minimum layer in these biochemical processes is not well understood (Toggweiler, 1989). This holds also for the relative importance of passive DOM release from particles, and for biological degradation through bacterial attack at intermediate water depths (Ishiwatari, 1992).

Nitrate and silicate concentrations are near zero at the sea surface and, particularly for nitrate, maximal in intermediate waters between 500 and 1500 m depth. The nitrate maximum and oxygen minimum are at approximately the same depth, and coincide with the salinity minimum of the Antarctic Intermediate Water south of latitude 20°N and the salinity maximum of the Mediterranean Water north of this latitude. Hence, oxygen and nitrate are closely connected to physical parameters that define the water masses of the intermediate zone. As with the physical parameters, their depth distribution seems to be connected to the large-scale advective transport of water masses.

Advective transport of water with high values of fluorescent matter is not obvious from the T/S data. These fluorescent molecules are produced *in situ* by a release from sinking particles in the upper thermocline, as found also in other oceanic regions (Momzikoff *et al.*, 1992).

The concept of sinking particles and their regeneration in this section of the water column agrees well with sediment trap measurements, which show that sinking particles are mostly degraded in the upper 200–300 m before they reach deeper waters (Martin *et al.*, 1987). This phenomenon was observed in the eastern Atlantic Ocean by Bishop *et al.* (1977, 1978), i.e. in the same regions where our fluorescence measurements were made.

Gelbstoff in intermediate and deep waters

At depths below a few hundred meters, and extending down to deep waters, the vertically and horizontally homogeneous distribution of gelbstoff fluorescence is a striking feature. The virtual constancy of the gelbstoff signal holds despite large variations in physical and chemical parameters at intermediate water depths. To describe this in more detail, a gelbstoff fluorescence–salinity diagram, which includes the data from all stations, was plotted (Fig. 5). Water masses are classified according to Emery and Meincke (1986) and labeled with individual symbols. For comparison with this figure, the depth profiles of gelbstoff fluorescence in Figs 2–4 are shown with the same symbols.

Data measured in the upper 500 m of the water column are shown with open symbols in the gelbstoff–salinity diagram. They are scattered over the diagram, taking on the lowest values of about $2\text{--}2.5 \times 10^{-3} \text{ nm}^{-1}$ Raman units at the sea surface of the South Atlantic Central Water (SACW). Below the surface layer the signal is between 3 and $5 \times 10^{-3} \text{ nm}^{-1}$ Raman units, and higher values belong to the maxima at 200–300 m depth discussed above. Salinity is higher in the Eastern North Atlantic Central Water (ENACW) than in the South Atlantic Central Water (SACW), but a specific difference in the Gelbstoff fluorescence intensity was not found.

Two intermediate waters at 500–1500 m depth are identified, the Antarctic Intermediate

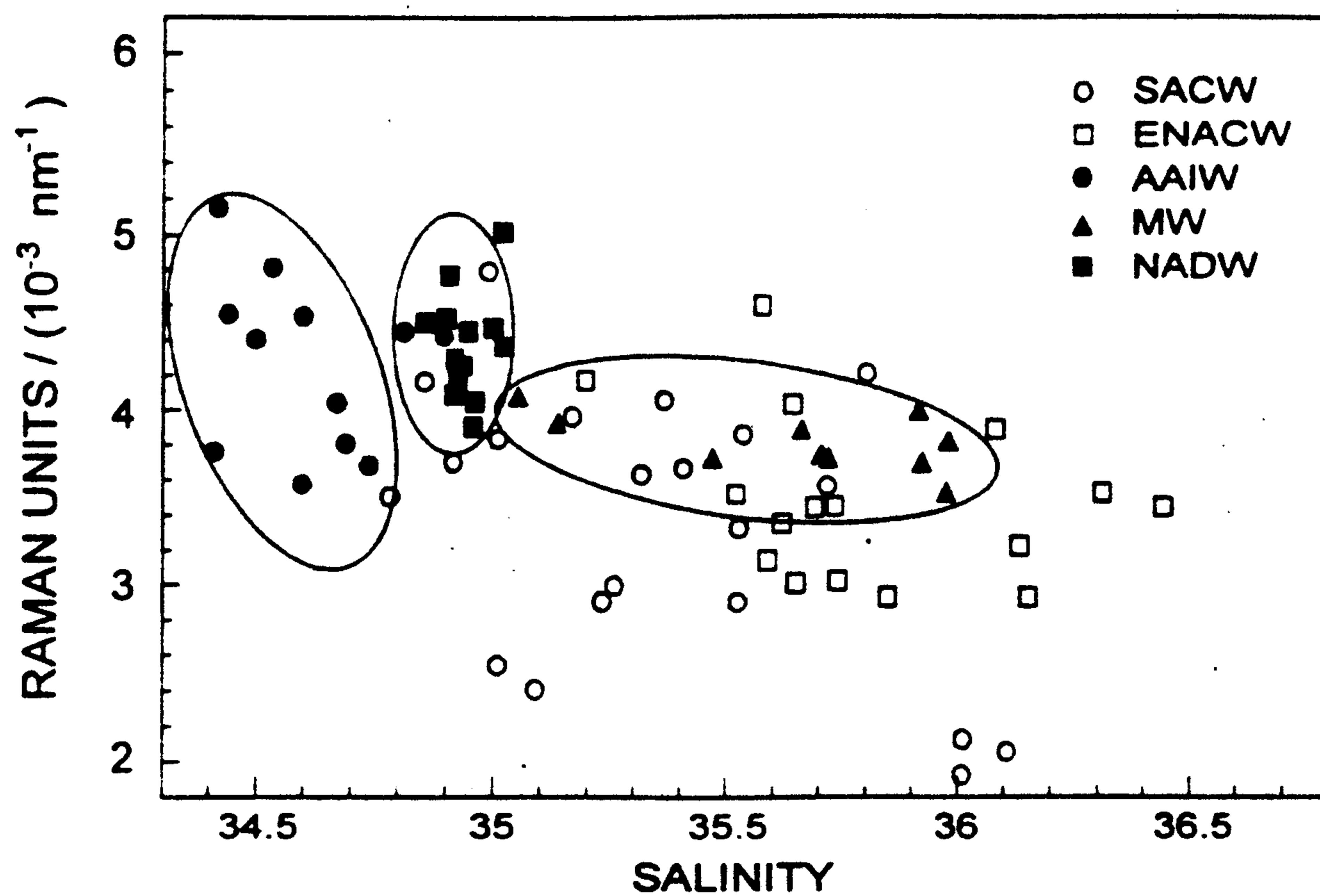


Fig. 5. Diagram of gelbstoff fluorescence vs salinity, data taken at the ANT-VIII/7 Stations, see Fig. 1 and Table 1. Individual symbols denote different water masses according to Emery and Meincke (1986), with the acronyms ENACW (Eastern North Atlantic Central Water), SACW (South Atlantic Central Water), AAIW (Antarctic Intermediate Water), MW (Mediterranean Water), NADW (North Atlantic Depth Water). Open symbols are used for samples taken from the upper water column, filled symbols for samples from intermediate and deep waters.

Water (AAIW) with $S < 34.8$ at Stas 588–592 (Fig. 2 and Fig. 3), and the Mediterranean Water (MW) with $S > 35.0$ at Stas 605 and 609 (Fig. 4). The intermediate water at Sta. 598 in the Cape Verde Basin, latitude 20°N , is a transition type between AAIW and MW; following the maps of Emery and Meincke (1986), the Eastern Atlantic Subarctic Intermediate Water is expected in this region, but a hydrographic classification based on our data is uncertain and was therefore omitted.

The AAIW is characterized by a relatively widespread salinity minimum and gelbstoff fluorescence ranging from 3.5 to $5.2 \times 10^{-3} \text{ nm}^{-1}$ Raman units. The highest fluorescence values are from 500 and 1000 m depth at Sta. 576, where the data differ considerably from the other profiles and would need to be verified. If these two data points are discarded, then the AAIW water mass fluorescence is 3.5 – $4.6 \times 10^{-3} \text{ nm}^{-1}$ Raman units.

Salinities of up to 36.0 at Sta. 605 mean that the core property of the MW, i.e. $S = 36.2$ in the outflow west of Gibraltar, was almost met. Fluorescence intensities of these samples are between 3.5 and $4.0 \times 10^{-3} \text{ nm}^{-1}$ Raman units.

North Atlantic Deep Water (NADW) is at depths below 1500 m, with $34.8 < S < 35.0$ and $1.5^{\circ}\text{C} < T < 4.0^{\circ}\text{C}$ (Emery and Meincke, 1986). The colder and less saline Antarctic Bottom Water is not observed, probably because of insufficient maximum depths of sampling. Like temperature and salinity, Gelbstoff fluorescence is limited to a small range between 3.9 and $4.8 \times 10^{-3} \text{ nm}^{-1}$ Raman units. The signal intensity is therefore slightly greater than in both types of intermediate waters lying on top of it. Mixing takes place between NADW and MW, where gelbstoff fluorescence behaves like a conservative property.

Profiles of tryptophan- and tyrosine-like substances

These depth profiles differ considerably from those of gelbstoff. Data taken near the sea surface show high concentrations of tryptophan-like molecules (Figs 2 and 3).

Photodegradation, a sink for gelbstoff fluorescence, is apparently less relevant for this fluorophore. The range of elevated tryptophan-like signals covers the entire mixed layer down to about 50 m. The maxima of gelbstoff fluorescence in the upper section of the main thermocline, i.e. at 200–300 m depth, are also apparent in most tryptophan and tyrosine profiles.

A fluorophor with maximum emission at 345 nm, when excited at 295 nm wavelength, was observed by Coble *et al.* (1990) in samples from the Black Sea; these authors associate the fluorophor with the indole ring of tryptophan. Mopper and Schultz (1993) report on a depth profile measured in the Sargasso Sea, with 210 nm excitation and 330 nm emission wavelength. They denote this signal as protein-like fluorescence. Despite the differences in the excitation wavelength, these signals are equivalent to what we call tryptophan-like fluorescence (Determann *et al.*, 1994). The distribution in the upper water column follows a pattern which is identical with our findings in the eastern Atlantic Ocean. Protein-like signals are strong within the mixed layer, and a second maximum is detected at 200 m depth in cases where humic-like signals are also at a high level.

According to our investigations of samples of phytoplankton and bacteria cultivated and analyzed in the laboratory, these particles do not emit fluorescence in the gelbstoff-dominated region of the spectrum. In contrast to this, the signals of aromatic amino acid fluorescence in the 280–350 nm region are more closely related to molecules bound to particles than to dissolved ones. Phytoplankton is a strong source of tryptophan-like fluorescence, as shown for *Phaeocystis* in Determann *et al.* (1994). Most probably the slightly shorter emission wavelength, as compared to the signature of free tryptophan, is due to the bound state of the amino acid, as discussed in the earlier paper. This holds also for bacteria, which emit fluorescence with maximum intensity at about 330 nm wavelength. These signals (Fig. 6) are sufficient to explain the signal intensity observed in the depth profiles (Figs 2–4).

The tyrosine-like fluorescence at 290 nm emission wavelength shows much less correspondence with horizontal variations of other seawater parameters (Determann *et al.*, 1994), and a well-defined relationship to particulate matter has not been found in our laboratory experiments. An explanation of this signal in terms of its source material is still open.

We therefore conclude that at least part of the tryptophan-like fluorescence reflects the presence of particulate organic matter. Phytoplankton abundances were very low during ANT-VIII/7 (Gröne and Karsten, 1991) and are not relevant for the data from below the photic zone. Therefore, the tryptophan-like depth profiles most probably describe the vertical distribution of tryptophan bound to bacteria.

CONCLUSIONS

The patterns of fluorescence versus depth in the eastern Atlantic Ocean are probably related to:

(i) the greater bacterial biomass in the upper 50 m, leading to the strongest tryptophan-like signal. This was virtually unaffected by photochemical degradation at the sea surface, which affects the gelbstoff fluorescence there;

(ii) lower tryptophan-like but high gelbstoff fluorescence in the water layer below the photic zone;

(iii) elevated tryptophan-like fluorescence in the 200–300 m layer on top of the main

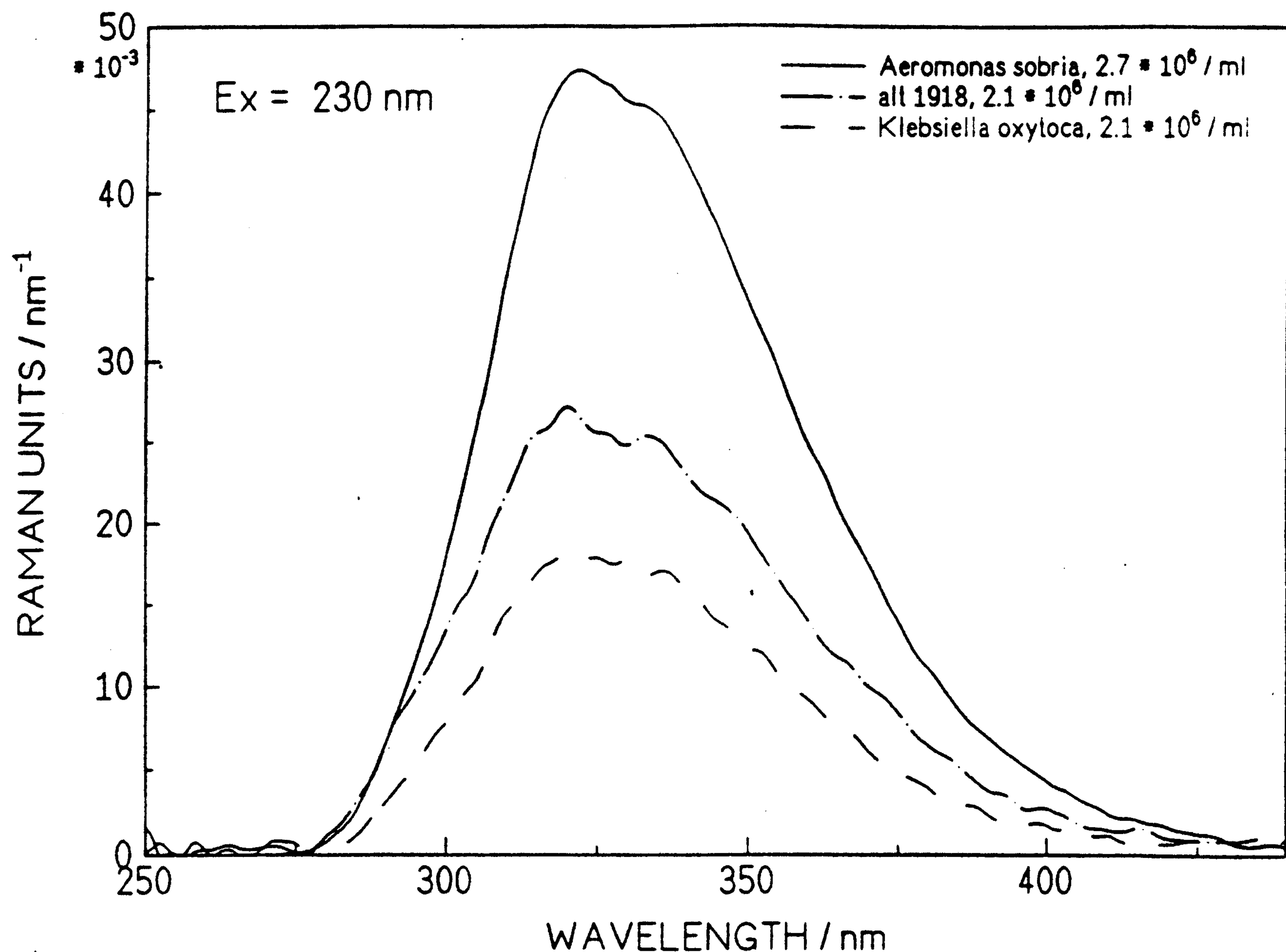


Fig. 6. Emission spectra of laboratory cultures of bacteria, 230 nm excitation. The fluorescence band around 330 nm is related to tryptophan bound to the bacteria. Cell numbers counted with a fluorescence microscope correspond to the upper range of typical open sea conditions near the sea surface. The sample alt 1918 was cultivated from a natural sample taken at 200 m depth near the Azores, 11th June 1983. To avoid background signals from the culture medium, bacteria were centrifuged five times at 10,000 rpm and resuspended in a 0.85% NaCl solution; this procedure was repeated five times. Residual background fluorescence and water Raman scattering of the NaCl solution was measured separately, and subtracted from the spectra.

thermocline, where both gelbstoff and tryptophan-like fluorescence may be enhanced due to particle degradation and bacterial activity related to this process; and

(iv) low tryptophan-like fluorescence in intermediate and deep waters where bacteria show low activity. Gelbstoff fluorescence is vertically homogeneous, the origin of this fluorophore being the advective transport of water masses. An important characteristic of this signal is its very low variability in view of the different origin of the intermediate and deep water masses in the eastern Atlantic Ocean.

Acknowledgements—We are grateful to the Alfred Wegener Institute for Polar and Marine Research, Bremerhaven, Germany, for making possible our participation in this cruise onboard R.V. *Polarstern*. Our thanks are due to the coordinator of the cruise Pr. O. Schrems and to the captain and the crew of the ship for their continuous help. We are indebted to Dr H.-J. Hirche, Alfred Wegener Institute, for making available the luminescence spectrometer for the measurements onboard R.V. *Polarstern*, to P. Wagner for his help in measuring the fluorescence data, to M. Schmidt for the quinine sulfate measurements, and to A. Michel for making available the unpublished hydrographic and chemical data measured during the cruise. We also thank Dr M. Mehrens and Dr S. Ullrich, Institute for Marine Research, Kiel, for their support in the optical analyses of marine bacteria. Participation in the cruise from Capetown to Bremerhaven was supported by grants from the Federal Minister of Research and Technology, Bonn.

REFERENCES

- Berger W. H. (1992) Global maps of ocean productivity. In: *Productivity of the ocean: present and past*, W. H. Berger, V.S. Smetacek and G. Wefer, editors, John Wiley, Chichester, U.K., pp. 429–455.
- Bishop J. K. B., J. M. Edmond, D. R. Ketten, M. P. Bacon and W. B. Silker (1977) The chemistry, biology and vertical flux of particulate matter from the upper 400 m of the equatorial Atlantic Ocean. *Deep-Sea Research*, **24**, 511–548.
- Bishop J. K. B., D. R. Ketten and J. M. Edmond (1978) The chemistry, biology and vertical flux of particulate matter from the upper 400 m of the Cape Basin in the southeast Atlantic Ocean. *Deep-Sea Research*, **25**, 1121–1161.
- Bristow M. and D. Nielsen (1981) Remote monitoring of organic carbon in surface waters. U.S. Environmental Protection Agency, Project Report EPA-60074-81-001, Las Vegas, NV, Feb. 1981, 83 pp.
- Chen R. F. and J. L. Bada (1992) The fluorescence of dissolved organic matter in seawater. *Marine Chemistry*, **37**, 191–221.
- Coble P., S. A. Green, N. V. Blough and R. B. Gagosian (1990) Characterization of dissolved organic matter in the Black Sea by fluorescence spectroscopy. *Nature*, **348**, 432–435.
- Coble P., R.B. Gagosian, F. Codispoti and C. Codispoti (1991) Dissolved fluorescence in the Black Sea. *Deep-Sea Research*, **38**, 958–1001.
- Determann S., R. Reuter, P. Wagner and R. Willkomm (1994) Fluorescent matter in the eastern Atlantic Ocean. Part I: Method of measurement and near-surface distribution. *Deep-Sea Research I*, **41**(4), 659–675.
- Dorsch J. E. and T. F. Bidleman (1982) Natural organics as fluorescent tracers of river–sea mixing. *Estuarine, Coastal and Shelf Science*, **15**, 701–707.
- Emery W. J. and J. Meincke (1986) Global water masses: summary and review. *Oceanologica Acta*, **9**, 383–391.
- Ertel J. R. (1990) Photochemistry of dissolved organic matter: An organic geochemical perspective. In: *Effects of solar ultraviolet radiation on geochemical dynamics in aquatic environments*, N.V. Blough and R.G. Zepp, editors. Woods Hole Oceanographic Institute Technical Report 90-09, pp. 79–81.
- Fütterer D. K. and O. Schrems, editors (1991) Reports on Polar Research. The Expedition ANTARKTIS-VII of R.V. "Polarstern" 1989/90. Reports of Legs ANT-VIII/6-7. Bremerhaven, 231 pp.
- Gröne T. and U. Karsten (1991) Bestimmung des Dimethylsulfoniumpropionat-Gehaltes (DMSP) im Phytoplankton. In: Reports on Polar Research. The expedition ANTARKTIS-VIII of R.V. "Polarstern" 1989/90. Reports of Legs ANT-VIII/6-7. Bremerhaven, pp. 197–202.
- Hayase K., M. Yamamoto, I. Nakazawa and H. Tsubota (1987) Behaviour of natural fluorescence in Sagami Bay and Tokyo Bay, Japan—vertical and lateral distributions. *Marine Chemistry*, **20**, 265–276.
- Hayase K., H. Tsubota and I. Sunada (1988) Vertical Distribution of fluorescent organic matter in the North Pacific. *Marine Chemistry*, **25**, 373–381.
- Heuermann R., K. D. Loquay and R. Reuter (1995) A multi-wavelength *in situ* fluorometer for hydrographic measurements. *Advances in Remote Sensing*, **3**(3), 71–77.
- Ishiwatari R. (1992) Macromolecular material (humic substance) in the water column and sediments. *Marine Chemistry*, **39**, 151–166.
- Ivanoff A. (1973) Facteurs physiques, chimiques et biologiques affectant la propagation de la lumière dans les eaux de mer. In: *Optics of the sea (interface and in-water transmission and imaging)*. North Atlantic Treaty Organization, Advisory Group for Aerospace Research and Development, AGARD Lecture Series No. 61. Technical Editing and Reproduction Ltd, London, p. 2.1-1–2.1-45.
- Kalle K. (1963) Über das Verhalten und die Herkunft der in den Gewässern und in der Atmosphäre vorhandenen himmelblauen Fluoreszenz. *Deutsche Hydrographische Zeitschrift*, **16**, 153–166.
- Kieber R. J., X. Zhou and K. Mopper (1990) Formation of carbonyl compounds from UV-induced photodegradation of humic substances in natural waters: Fate of riverine carbon in the sea. *Limnology and Oceanography*, **35**, 1503–1515.
- Kouassi A. M. and R. G. Zika (1990) Light-induced alteration of the photo-physical properties of dissolved organic matter in seawater. Part I. Photoreversible properties of natural water fluorescence. *Netherlands Journal of Sea Research*, **27**, 25–32.
- Kouassi A. M., R. G. Zika and J. M. C. Plane (1990) Light-induced alteration of the photophysical properties of dissolved organic matter in seawater. Part II. Estimates of the environmental rates of the natural water fluorescence. *Netherlands Journal of Sea Research*, **27**, 33–41.
- Kramer C. J. M. (1979) Degradation by sunlight of dissolved fluorescing substances in the upper layers of the eastern Atlantic Ocean. *Netherlands Journal of Sea Research*, **13**, 325–329.

- Martin J. H., G. A. Knauer, D. M. Karl and W. W. Broenkow (1987) VERTEX: carbon cycling in the northeast Pacific. *Deep-Sea Research*, **34**, 267–285.
- Michel A. (1991) Nährstoffe und CTD-Daten. In: Reports on Polar Research. The Expedition ANTARKTIS-VIII of R.V. "Polarstern" 1989/90. Reports of Legs ANT-VIII/6-7. D.K. Fütterer and O. Schrems, editors. Bremerhaven, pp. 214–217 and pp. 224–225.
- Momzikoff A., S. Dallot and M.-E. Pizay (1992) Blue and yellow fluorescence of filtered seawater in a frontal zone (Ligurian Sea, northwest Mediterranean Sea). *Deep-Sea Research*, **39**, 1481–1498.
- Mopper K. and C. A. Schultz (1993) Fluorescence as a possible tool for studying the nature and water column distribution of DOC components. *Marine Chemistry*, **41**, 229–238.
- Mopper K., X. Zhou, R. J. Kieber, D. J. Kieber, R. J. Sikorski and R. D. Jones (1991) Photochemical degradation of dissolved organic carbon and its impact on the oceanic carbon cycle. *Nature*, **353**, 60–62.
- Nyquist G. (1979) Investigation of Some Optical Properties of Seawater with Special Reference to Lignin Sulfonates and Humic Substances. Ph.D. Thesis, Göteborgs Universitet, 200 pp.
- Toggweiler J. R. (1989) Is downward DOM flux important in carbon transport? In: *Productivity of the ocean: present and past*, W.H. Berger, V.S. Smetacek and G. Wefer, editors, John Wiley, Chichester, U.K., pp. 65–83.

APPENDIX: DEPTH PROFILE DATA

Depth (m)	T (°C)	S	Fluorescence 10^{-3} Raman units (nm^{-1})			O ₂ (ml l^{-1})	NO ₃ ⁻ ($\mu\text{mol l}^{-1}$)	Si(OH) ₄ ($\mu\text{mol l}^{-1}$)	Water Mass
			Excitation/Emission 254/440	Wavelength 270/320	230/290				
Station 576									
5	20.51	35.32	2.5	6.6	—	5.27	—	—	SACW
20	20.04	35.25	2.4	8.2	—	5.26	0.30	2.62	...
50	16.49	35.43	3.6	7.2	—	5.28	4.41	2.53	...
70	15.45	35.42	3.0	4.5	—	5.17	9.31	3.64	...
100	14.77	35.35	2.9	5.5	—	4.73	8.70	5.14	...
200	12.35	35.06	2.5	3.3	—	4.87	13.89	6.95	SACW
300	10.06	34.75	3.5	3.2	—	4.60	16.72	10.43	AAIW
500	5.90	34.40	5.2	3.4	—	4.41	27.96	22.18	...
1000	3.45	34.54	4.8	4.9	—	3.98	33.34	20.64	AAIW
1500	3.18	34.81	4.4	3.3	—	4.68	26.63	47.71	NADW
2000	2.95	34.89	—	12.4	—	5.22	23.70	44.09	...
3000	2.22	34.88	6.3	13.7	—	5.41	34.31	58.29	NADW
Station 582									
5	—	—	2.0	6.7	—	—	—	—	SACW
20	24.10	36.71	2.1	5.3	—	4.71	0.49	2.73	...
50	16.52	35.74	3.8	6.5	—	3.95	1.94	2.21	...
100	13.02	35.29	3.7	3.2	—	2.19	24.06	9.68	...
200	10.90	35.02	4.8	3.7	—	1.45	28.80	16.18	SACW
300	9.54	34.89	4.2	4.2	—	1.04	46.34	16.97	AAIW
500	7.05	34.65	4.6	3.6	—	1.30	49.13	23.62	...
1000	3.95	34.59	4.5	6.7	—	3.56	34.50	30.94	AAIW
1500	3.61	34.90	4.4	3.9	—	4.67	35.89	31.68	NADW
2000	3.13	34.92	4.3	2.9	—	5.15	29.71	33.76	...
3000	2.30	34.91	4.5	2.5	—	5.21	28.22	50.65	...
3500	2.10	34.90	4.5	2.6	—	5.23	28.26	57.69	NADW
Station 588									
5	19.45	—	2.4	8.0	4.3	4.81	—	—	SACW
20	17.69	35.95	3.6	6.0	2.6	4.42	4.96	5.01	...
50	15.24	35.61	3.3	5.1	4.9	3.64	11.90	5.24	...
70	15.03	35.55	2.9	4.4	3.0	3.69	10.07	5.91	...

Depth (m)	<i>T</i> (°C)	<i>S</i>	Fluorescence 10^{-3} Raman units (nm^{-1})			O_2 (ml l^{-1})	NO_3^- ($\mu\text{mol l}^{-1}$)	Si(OH)_4 ($\mu\text{mol l}^{-1}$)	Water Mass
			Excitation/Emission Wavelength						
			254/440	270/320	230/290				
100	14.54	35.48	3.7	4.6	2.5	3.24	10.69	7.30	SACW
200	12.07	35.16	4.4	5.8	4.7	2.10	15.39	10.79	AAIW
300	9.00	34.83	3.6	3.4	2.9	1.99	20.47	18.52	...
500	6.13	34.56	3.8	3.0	3.1	3.06	21.40	25.54	...
1000	4.33	34.69	3.8	4.0	8.6	3.69	20.07	37.49	...
1500	4.05	34.96	4.0	4.9	25.9	5.29	13.35	22.31	NADW
2000	3.36	34.98	3.9	3.4	6.4	5.77	12.72	23.69	...
3000	2.40	34.92	4.6	5.2	2.7	5.57	22.00	46.90	NADW
Station 592									
5	25.18	36.01	1.9	7.7	4.0	4.91	—	—	SACW
20	19.98	36.01	2.1	7.8	4.5	4.68	0.19	1.58	...
50	15.95	35.80	4.2	5.8	5.9	2.70	19.25	3.87	...
100	14.59	35.54	3.9	3.9	2.7	1.63	34.89	8.16	...
200	12.07	35.37	4.1	3.9	2.3	2.36	39.11	10.13	...
300	9.93	35.17	4.0	5.0	3.5	1.44	50.70	13.09	SACW
500	7.31	34.74	3.7	3.0	2.6	2.15	63.39	21.74	AAIW
1000	4.74	34.67	4.0	2.7	5.4	3.09	65.18	33.41	AAIW
1500	3.94	34.92	4.1	2.6	9.0	4.53	54.11	25.02	NADW
2000	3.24	34.94	4.3	3.6	5.4	5.11	50.40	27.00	...
3000	2.43	34.91	4.8	3.3	5.4	5.35	53.04	41.37	...
4800	1.81	34.86	4.5	3.9	9.0	5.61	50.82	58.77	NADW
Station 598									
50	18.14	36.54	3.5	7.9	12.1	4.36	7.50	10.14	ENACW
70	17.23	36.33	3.2	4.6	10.1	3.77	11.25	5.00	...
100	16.47	36.15	3.9	5.1	18.0	2.88	17.50	7.25	...
200	13.81	35.67	4.0	3.7	16.0	1.69	16.05	11.66	...
300	12.68	35.59	4.5	3.9	5.1	1.28	22.24	15.58	...
500	9.96	35.25	4.2	3.3	6.5	1.41	28.57	10.14	ENACW
1000	6.27	34.99	4.0	3.8	4.0	2.66	31.94	24.97	NADW
1500	4.47	35.05	4.4	2.4	1.7	4.56	27.46	25.14	...
2000	3.49	35.00	4.5	2.5	12.4	4.82	22.86	28.42	...
3000	2.51	34.94	4.2	3.1	53.5	5.47	23.01	39.79	NADW
Station 605									
50	15.25	36.19	2.9	9.3	4.7	5.46	—	0.28	ENACW
100	14.70	36.11	2.9	5.5	3.0	5.35	—	1.04	...
200	12.78	35.79	3.5	5.8	5.1	5.09	—	3.82	...
300	11.92	35.65	3.4	3.1	2.2	5.02	—	4.80	ENACW
500	11.31	35.59	3.7	3.0	1.9	4.48	—	6.12	MW
750	10.87	35.96	3.5	2.6	1.8	4.49	—	9.77	...
1000	10.40	36.02	3.8	2.7	1.8	4.41	—	11.10	...
1250	8.99	35.99	4.0	2.8	1.0	4.62	—	12.43	...
1500	6.55	35.57	3.7	2.5	2.2	5.12	—	14.43	...
2000	3.84	35.11	4.1	2.8	1.6	5.50	—	21.79	MW
3000	2.42	34.93	4.2	2.3	1.7	5.60	—	41.22	NADW
4000	2.09	34.89	4.4	2.3	1.7	5.56	—	56.01	NADW
Station 609									
50	12.82	35.74	3.0	9.1	3.6	6.10	7.22	1.21	ENACW
100	12.64	35.72	3.4	5.0	2.8	5.87	3.51	1.49	...

Depth (m)	<i>T</i> (°C)	<i>S</i>	Fluorescence 10^{-3} Raman units (nm^{-1})			O_2 (ml l^{-1})	NO_3^- ($\mu\text{mol l}^{-1}$)	Si(OH)_4 ($\mu\text{mol l}^{-1}$)	Water Mass
			Excitation/Emission Wavelength						
			254/440	270/320	230/290				
200	12.08	35.65	3.0	3.8	1.7	5.74	7.41	2.09	...
300	11.64	35.59	3.1	3.4	2.0	5.64	10.71	3.02	...
500	10.83	35.52	3.5	3.0	2.0	5.17	14.16	4.91	ENACW
750	10.49	35.70	3.7	2.8	2.2	4.48	19.46	8.41	MW
1000	10.62	35.95	3.7	2.5	1.6	4.30	21.55	9.34	...
1250	8.43	35.64	3.9	2.6	1.3	4.62	23.71	11.56	...
1500	5.32	35.14	3.9	3.2	2.0	5.43	25.04	12.92	MW
2000	3.86	35.01	5.0	4.8	2.9	5.91	20.86	18.92	NADW
3000	2.76	34.95	4.4	2.7	1.7	5.78	17.41	35.67	...
4600	2.50	34.90	4.6	3.9	2.6	5.62	13.79	48.24	NADW